A Plane Wave Generator Based on the Design Principles of a Compact Antenna Test Range

C.G. Parini[2] R.F. Dubrovka[2] S.F. Gregson[1, 2]
[1] Next Phase Measurements LLC, CA, USA, stuart.gregson@qmul.ac.uk
[2] Queen Mary University London, London, UK

***Abstract*—The use of plane-wave generators (PWG) for antenna measurements in a production-line environment is becoming a popular choice, as they offer a highly compact solution to producing a pseudo plane-wave in the near-field (termed Quiet Zone) in which the Antenna Under Test (AUT) can be placed. However, they are costly to construct as they generally need a large number of digital amplitude and phase shifters to control the array of radiating elements that form the PWG. In this paper we design a PWG based on the design principles of a Compact Antenna Test Range (CATR) which requires only a few digital amplitude controllers and no digital phase shifters to achieve a performance compatible with that of a CATR.**

***Index Terms*—antennas, antenna measurements, plane-wave generators.**

I. INTRODUCTION

The measurement of antenna radiation patterns and other parameters such as gain, impedance, EIRP etc. can be split into three distinct categories: (i) Direct measurement of the Antenna Under Test (AUT) at a suitable far-field distance; (ii) Direct measurement using a pseudo plane-wave created by some source much closer than the far-field distance, for example a Compact Antenna Test Range (CATR); (iii) By measuring the AUT radiation in the near-field with a probe antenna that is scanned over a suitable canonical surface and mathematically transforming this data to the far-field, for example Spherical Near-Field (SNF) measurement. In the field of production testing of antennas the second category, epitomised by the CATR, offers many advantages including: (i) A compact enclosed facility free from outside RF interference that can be fitted into a factory environment; (ii) Fast and direct measurement of radiation characteristics without the need for lengthy field probing over a suitable surface and time-consuming post processing, as well as the ability to determine the performance when testing with complex waveforms, e.g. for OTA type testing. The first practical implementation of the classic point-source single offset reflector based CATR dates back to Johnson [1], working at Georgia Institute of Technology in 1975. Subsequently the CATR has developed as an industry standard taking many forms and coving a very wide range of microwave and millimetrewave frequencies, a review of which can be found in chapter 5 of [2]. A more recent alternative to the CATR is the Plane Wave Generator (PWG), first reported in 1988 [3], where an array of antennas is used to synthesise a plane-wave in the near-field. In both cases the 'plane-wave' region is defined by the Quiet Zone (QZ), with an industry standard definition of a region where the amplitude and phase ripple is less than ±0.5dB and ±5° respectively, and the amplitude taper across the region is <1dB [2]. The advantage of the PWG over the CATR is that its physical size can be kept smaller thus reducing the cost of the anechoic chamber and host building required to enclose these facilities. However, its main disadvantages are the complexity, RF loss, and cost of the requisite RF beam forming network which typically limits its use to frequencies <30GHz and its limited instantaneous bandwidth. Commercial PWG systems exist in the 1-6 GHz band, for example [4] with QZ size of 500mm diameter and [5] with QZ size of 480mm diameter.

The classical design of PWG controls both the amplitude and phase excitation of the array, where the weighting coefficients are calculated using methods, such as the least square (LS), singular value decomposition (SVD), and sparse optimization algorithms to achieve the desired QZ amplitude and phase ripple [6]. It is noted in [7] that using these traditional regression approach, electric field intensity outside the QZ might be significantly greater than that inside the quiet zone, which would inevitably cause high wall illumination and increase scattered fields entering the quiet-zone region. The approach in [7] uses a more complex synthesis process using several regions to define the QZ and results in the percentage of energy from the PWG radiated in QZ being 44% compared to just 8% when using a simple LS method. The above reviewed PWG systems all require complex excitations utilising both amplitude and phase weights for the array elements of the PWG, leading to a costly beamforming network behind the array and complex calibration process. In [8] a design of PWG using just amplitude weights with a constant plane phase across the array is described. This 16 x 16 array of quad ridge waveguide elements uses subarrays to simplify the feeding leading to just 16 amplitude weights to determine the QZ. In addition, the elements are spaced in a non-uniform way to support wideband operation. QZ amplitude and phase variation up to ±1.25 dB and ±7.5°, respectively, is achieved in the measured results for frequencies ranging from 2.4 to 5 GHz. However, we note the QZ amplitude ripple significantly exceeds the desired ±0.5dB CATR, which will result in compromised antenna measurements. The use of a nonuniform PWG array element spacing is taken forward in [9] where elements are placed around rings of different (nonuniformly spaced) radii with varying numbers of elements used within each ring. Compressive sensing is employed to determine this sparse

PWG array geometry. With a uniform phase excitation across the 83-element array, each of the 8 rings form a subarray which is fed with amplitude only weights which change with frequency. These 8 weights are obtained iteratively to maximize the radiated power inside the QZ sphere as well as minimizing the amplitude and phase ripple. For the 600mm diameter QZ, the amplitude and phase ripple obtained through simulation, over 2.4GHz to 5GHz, was 0.96dB and 8.1° respectively. The concept of defining the QZ over a sphere is also addressed in [10] which proposes a hybrid combination of Least Squares and Genetic Algorithm approaches to obtain the amplitude and phase weights of an 8 x 8 PWG with ideal point sources. An empirical formulation to determine the required minimum number of PWG radiating elements for a given QZ size and location is presented in [11], which uses an information transmission rate analysis method based on the singular value decomposition (SVD) of the PWG to AUT transfer matrix. A more extensive set of PWG design guidelines, including a similar formulation for size can be found in [12]. A general rule of thumb is that the QZ is typically half the size of the PWG and is located at a distance equal to the size of the PWG, which is approximately the rule of thumb commonly used in the design of traditional CATRs relating the reflector size to QZ dimensions.

Considering now the types of PWG radiating element, [13] proposes an absorber-integrated tapered slot antenna offering low VSWR and low structural RCS. The Vivaldi / tapered slot antenna is a popular PWG element candidate as it offers wide bandwidth, comparatively low manufacturing costs and reasonable power handling. Examples of dielectric and absorber loaded designs are described in [14,15].

In this paper we describe the design of a low cost PWG that is to be used in a production environment to test Massive Multiple Input Multiple Output (MIMO) antenna EIRP in the 3.5GHz band. To keep costs low we have taken the uniform phase approach and used our experience with CATR design to derive a simple initial amplitude excitation of the array that employs a uniformly illuminated central region combined with a taper to the edges of the PWG and makes extensive use of sub-arraying to minimize the required number of digital amplitude controllers. The PWG of size 11 x 11 employs dual polarised Vivaldi antenna elements and has an overall dimension of 1m x 1m. In section II we describe the Vivaldi antenna element and section III describes the PWG design philosophy. Section IV describes the simulated results for the PWG design and the simulated results of "measuring" a 6 x 8 element MIMO antenna tile in the PWG. Conclusions are presented in section V.

II. DUAL POLARISED VIVALDI ANTENNA

As described above in Section I, the Vivaldi antenna presents an attractive design for the PWG array element offering a wide bandwidth and simple low-cost construction using double-sided high-frequency, low-loss microwave substrate. The design employed here follows the usual Vivaldi design process [14,15] yielding an antenna of height 169.5mm and 80mm square base (which is covered with absorber) with the two Vivaldi vanes orientated at ±45° to give the two polarisations of ±45° to the x-y axes of the 11 x 11 array.

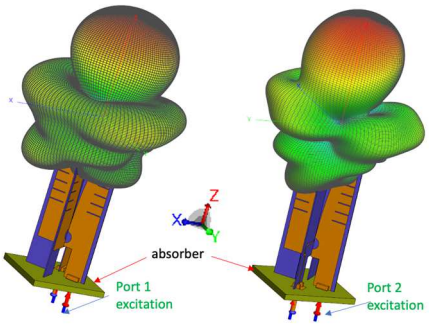

Fig. 1. Radiation patterns of isolated dual-polarised Vivaldi array element for the +45° and -45° polarisations.

A FEKO full-wave model of the element was constructed, and the isolated element radiation pattern at 3.5GHz is shown in Fig. 1 for both hands of polarisation generated from feeding ports 1 and 2. The 3.5GHz input reflection coefficients for ports 1 and 2 was found to be -18.2 dB and -19.4 dB respectively. The cross-coupling between the ports was found to be <-34 dB. The gain of the isolated element for ports 1 and 2 was found to be 9.24dB and 8.1dB respectively. Vivaldi antennas are renowned for their broadband operation with this radiator offering useable performance from 2.5 to 5.0 GHz.

III. PWG DESIGN

As stated in the introduction, our aim was to design a compact PWG that can measure the EIRP of a massive MIMO antenna tile comprising 6 x 8 radiating elements which has the dimension of approximately 0.36m square. We thus defined the QZ size to be 0.42m square to give a design margin, the operating frequency of the PWG was centred on 3.5GHz We start the design using the desired geometry of the PWG system shown in Fig. 2 (bottom right).

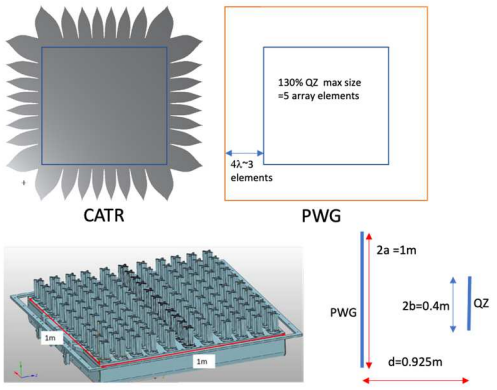

Fig. 2. Top: Equivalence of CATR reflector and PWG aperture of size 11 x 11 elements. Bottom left: Vivaldi antenna element based 11 x 11 PWG; Bottom right: dimensions of PWG system.

We then determine the minimum number of PWG element using the empirical formula from [11] reproduced here in (1).

$$N = int\left[\frac{2}{\lambda}(R_1 - R_2) + 5\right] \quad (1)$$

Where $R_1 = \sqrt{(a+b)^2 + d^2}$, $R_2 = \sqrt{(a-b)^2 + d^2}$. Applying (1) to the geometry shown in Fig. 2 suggests the minimum size of the array should be 9 x 9. We have taken an extra ring of elements to allow a design margin, resulting in a PWG array size of 11 x 11 elements.

As noted within the introduction, our aim was to design a low cost PWG solution and so a uniform phase design was chosen which requires no digital phase shifters keeping costs low and removing undesirable amplitude errors associated with transmission through the phase shifter. Initial phase calibration of the array using a planar scanner and probe would use SMA line-stretchers at each feed to achieve the desired uniform phase excitation. To address the amplitude excitation of the PWG elements, we wanted to make maximum use of subarrays to keep the digital attenuator count as low as possible. In Fig. 2 we consider the duality between designing a CATR to that of designing a PWG. Both have a uniform amplitude central region to the radiating aperture, which for a CATR would be about 130% of the QZ dimension and its inclusion is essential to the success of the design. For the PWG this would represent a central region of 5 x 5 elements which could all be feed from a power splitter. The outer ring of array elements which is 3 elements wide then needs to have a tapered amplitude which for a CATR is often achieved through the use of castellations [2]. For the PWG, we used as a starting point to have the 3 rows and 3 columns shown in Fig. 3 (top) to have an amplitude taper defined by $\sin^{1.6}$ across the width of the rim which is a commonly used target "window" in CATR serration design.

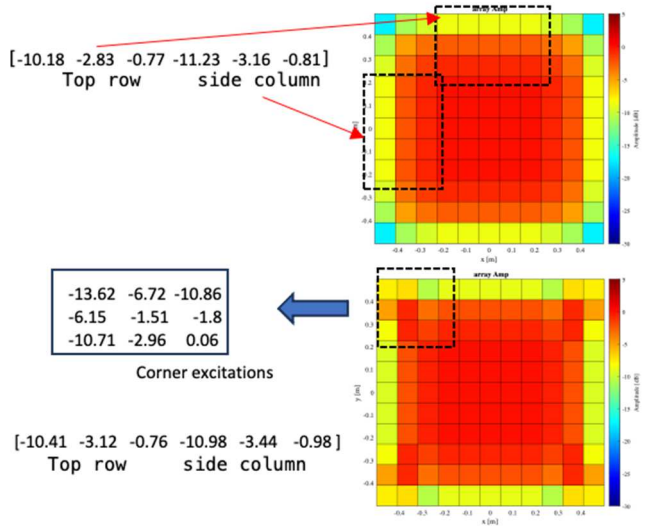

Fig. 3. Top: Optimised design using row and column amplitude excitations giving 6 coefficients to define array. Bottom: 9 additional coefficients to determine the corner element excitations, giving a total of 15 coefficients to define array. PWG element seperation = 100mm

For the 3 x 3 corner elements the amplitude was obtained by multiplying the row amplitude with the column amplitude at each of the 9 corner elements. This led to the PWG amplitude excitation similar to that shown in Fig. 3 (top). Such a design could be implemented with just 6 digital attenuators (3 for the row elements and 3 for the column elements) plus RF amplitude multipliers for the corner elements. To test this design a MATLAB model of the PWG array was developed which used the radiation pattern of the Vivaldi elements obtained using the FEKO model of section II to derive the QZ amplitude and phase. Results for this are presented in the next section.

As an alternative to the initial $\sin^{1.6}$ excitation we used a Genetic Algorithm (GA) to determine the optimal 6 amplitude excitations (3 for the rows and 3 for the columns, as shown in Fig. 3) with the aim to minimise the amplitude and phase ripple in the QZ. Here, the minimisation objective function being that shown in (2) using 6 coefficient optimisation, which we have termed *opt6*. This penalty function was adopted as it offers equal priority to both amplitude and phase ripple as the target QZ is peak-to-peak amplitude and phase ripple of 1dB and 10° respectively.

$$\textit{amplitude ripple (dB)} + \textit{(phase ripple (degs))/10} \quad (2)$$

A second GA optimisation design, which added optimisation of the amplitude of the 9 corner elements to the above 3 row and 3 column case, was implemented and is therefore 15 optimisation terms (termed *opt15*), which is illustrated in Fig. 3 (bottom). As stated in Section I, an additional figure of merit for the PWG could be the percentage of the power radiated by the PWG that reaches the QZ, which needs to be as high as possible to avoid too much power illuminating the walls of the anechoic chamber and then finding its way back into the QZ. In the next section we take these various design options and model the QZ amplitude and phase ripple as well as the percentage of total power that is transmitted to the QZ.

IV. PWG SIMULATED PERFORMANCE

A. *Quiet Zone performance*

In this section we take the MATLAB model of the PWG with Vivaldi elements and compare the QZ performance for the various design options considered in the previous section. However, we first consider the performance of the PWG array using the radiation pattern of the isolated array element (fig. 1.) using two different array element spacings of 100mm and 90.9mm. Table I. summarises the results of the amplitude and phase ripple over the QZ of 0.42m square.

TABLE I. QZ PK-PK AMPLITUDE AND PHASE RIPPLE FOR DIFFERENT RIM AMPLITUDE DESIGNS OF 11 X 11 PWG. QZ SIZE = 0.42M SQUARE. S = ARRAY ELEMENT SEPARATION

Rim element amplitude excitation	Pk-pk amplitude ripple (dB) S= 100mm	Pk-pk Phase ripple (degrees) S= 100mm	Pk-pk amplitude ripple (dB) S= 90.9mm	Pk-pk Phase ripple (degrees) S= 90.9mm
Sin^1.6	0.81	14.1	1.6	18.7
Row and column optimized (6 terms)	0.65	9.2	0.67	10.9
Row, column and corner optimized (15 terms)	0.94	6.0	0.57	11.5

For the wider element separation, the $\sin^{1.6}$ excitation is quite close to providing an acceptable amplitude and phase ripple in the QZ. However, reducing the separation to 90.9mm

results in very poor amplitude ripple and trying powers other than 1.6 offered no significant improvement. Moving to the opt6 results both array sizes show acceptable QZ ripple. For the opt15 case the 100mm spaced array shows higher (but acceptable) amplitude ripple. Not surprisingly, the array separation is a critical factor in determining the QZ field. An example of the field from the PWG over a 4m x 4m plane at the QZ distance of 0.925m is shown in Fig. 4 for the case of opt6 and 100mm separation, with the white square on the plots showing the QZ region.

Clearly the proposed design concept is viable, and to better evaluate the performance we remodelled the Vivaldi antennas using a periodic boundary condition model option in FEKO to better model the element's radiation pattern when embedded within an array, to approximately take into account mutual coupling effects within the array.

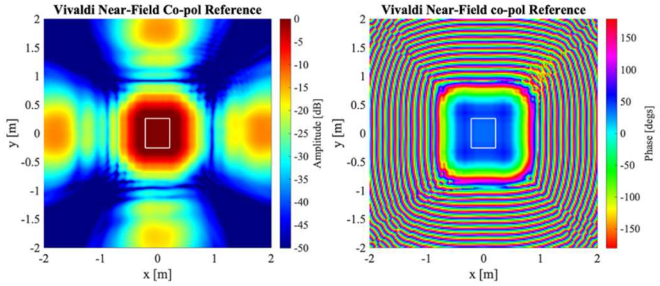

Fig. 4. Co-polar field over QZ plane (4m x 4m) for +45° polarized isolated Vivaldi 11 x11 PWG using amplitude excitation of figure 3(top). QZ X-polar peak of -20.7dB. Element separation = 100mm, amplitudes obtained from 6 coefficient optimization. White square shows the QZ region.

The embedded element radiation pattern for both hands of polarisation is shown in Fig. 5. In this case the input reflection coefficients for ports 1 and 2 was found to be -16.1 dB and -11.5 dB respectively with the cross-coupling between the ports remaining <-38 dB.

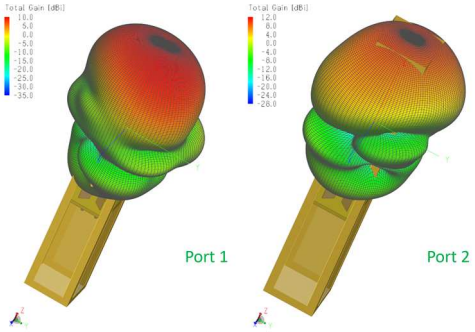

Fig. 5. Radiation patterns of embedded Vivaldi array element for the +45° and -45° polarisations.

Table II. compares the PWG performance for both 6 and 15 term optimisation coefficients, and for both polarisations (port 1 and port 2) for the QZ size that offers amplitude and phase ripple better than ±0.5dB and ±5°. There is little difference between the 6 and 15 term optimisation results, with the 15-term case offering only a slightly larger QZ. Using the isolated radiation pattern of the Vivaldi antenna predicts a better performance but the embedded pattern is the more realistic model. Only about 20% of the power from the PWG enters the QZ and the peak cross-polarisation in the QZ is significantly better for port 1 over port 2, mainly due to off-axis x-polar level being higher for port 2.

TABLE II. PERFORMANCE SUMMARY OF ±45° POLARIZED VIVALDI PWG ELEMENT SPACING 100MM

Vivaldi element	QZ width (m)	QZ height (m)	QZ Pk-pk Amplitude ripple (dB)	QZ Pk-pk phase ripple (degrees)	Maximum QZ x-polar amplitude (dB)	% total power through QZ
Isolated port 1 (0pt6)	0.43	0.51	0.56	9.8	-20.7	32.7
Isolated port 2 (0pt6)	0.51	0.51	0.82	9.7	-22.3	31.7
Embedded port 1 (0pt6)	0.43	0.43	0.47	10.0	-28.8	21.3
Embedded port 2 (0pt6)	0.43	0.43	0.60	10.0	-21.8	15.3
Embedded port 1 (0pt15)	0.47	0.47	0.77	9.2	-27.8	23.6
Embedded port 2 (opt15)	0.43	0.51	0.96	7.7	-20.6	16.8

An example of the field from the PWG over a 4m x 4m plane at the QZ distance of 0.925m is shown in Fig. 6 for the case of port 1 and *opt15*, with the white square on the plots indicating the QZ region.

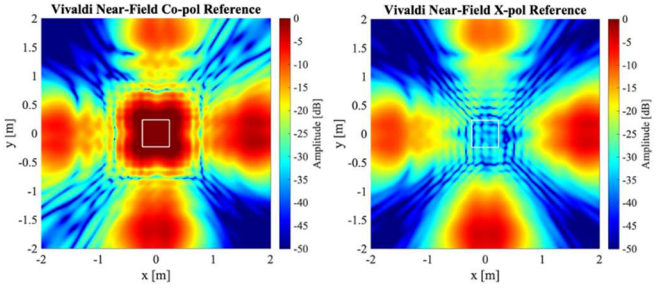

Fig. 6. Co-polar and X-polar QZ field for port 1 (+45° polarized) embedded Vivaldi 11 x11 PWG opt15 and Element separation = 100mm. QZ x-polar peak of -27.8dB. White square shows the QZ region.

One disadvantage of this design approach is the comparatively low percentage of the transmitted power from the PWG that enters the QZ, meaning that a full anechoic chamber must be used to enclose the test chamber. However, in a production-line environment test facility a fully screened anechoic chamber for the PWG is a necessity to avoid RF interference between adjacent test sites.

To assess the manufacturing tolerances for the PWG we first considered what accuracy was required for the x-y placement of the Vivaldi feeds in the array. Using a random x-y location error with peak of ±1mm for each element in the array the resulting QZ amplitude and phase ripple increased from 0.96dB and 7.7° to 1.01dB and 8.0°, which is negligible. For the case of a random z location error with peak of ±1mm for each element in the array the resulting QZ amplitude and phase ripple increased to 1.34dB and 9.5°, which in terms of amplitude ripple is significant, suggesting a tolerance of better than ±1mm is required for element z location.

For tolerance on the levels of amplitude excitation we took the opt15 case and changed the amplitudes across all 121 elements randomly with a peak error of ±0.5dB, the QZ amplitude and phase ripple increased from 0.96dB and 7.7° to 1.19dB and 9.3°, confirming that amplitude excitation errors need to be kept below ±0.5dB.

B. *Simulated results of "measuring" MIMO antenna in the PWG*

In this subsection we take the PWG opt6 embedded element pattern results for the QZ and compute the radiation pattern that would be "measured" for a 6 x 8 element MIMO antenna as the AUT. To undertake this task, we use a model of a simple 6 x 8 element square patch element as the AUT and compute the near-field (all six E- and H-field components) over the surrounding complete sphere of radius 0.75m centred at the AUT origin. We then repeat this process over the exact same sphere computing the field from the PWG and use the Power Coupling Theorem [16] to determine the coupling between the two antennas. We then repeat the field calculation for the AUT orientated at different azimuth and elevation positions to determine the "measured' radiation pattern of the AUT.

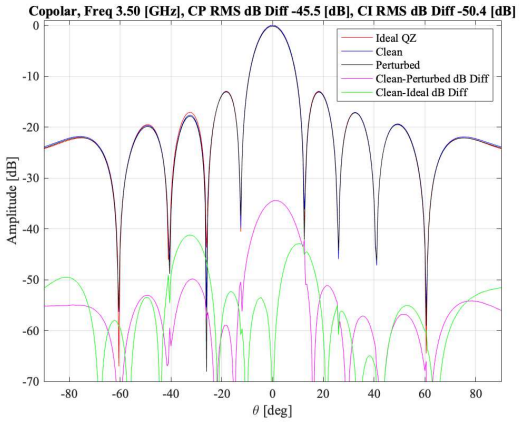

Fig. 7. 'Measured' radiation pattern of 8 x 6 element array AUT for ideal QZ, 'clean' PWG QZ, 'perturbed' PWG QZ. Difference patterns 'clean' to 'pertubed' and 'clean' to 'ideal' are shown in magenta and green respectively

Fig. 7 shows a typical azimuth pattern cut comparing the "measured" (clean) and theoretical (ideal) AUT radiation pattern along with the difference pattern. The 'measurement' is then repeated with the perturbed QZ where PWG elements are subject to a random z location error of maximum ±1mm and random amplitude weight error of maximum ±0.5dB which has a QZ amplitude and phase ripple of 1.45dB and 10.7° respectively. The Boresight EIRP uncertainty between the 'clean' and 'perturbed' QZ is 0.16dB which is a little high and emphasizes the importance of keeping the QZ amplitude and phase ripple down to ±0.5dB and ±5°.

V. CONCLUSIONS

This paper demonstrates that a 'simple' PWG can be constructed based on an array with uniform phase excitation and as little as six variable amplitude weights combined with sub-arraying and an RF amplitude multiplier to feed all 121 array elements. Alternatively, 15 variable amplitude weights and no RF multiplier can be used. Both systems offer a QZ amplitude and phase ripple of ±0.5dB and ±5°. We have shown through simulated measurement of a 6 x 8 MIMO array antenna pattern the importance of the z location of the PWG array elements as well as the need to maintain the accuracy of the amplitude weights to better than ±0.5dB.

REFERENCES

[1] Johnson R.C., 'Performance of a compact antenna range', Antennas and Propagation Society International Symposium. 1975;13:349–52.

[2] C.G. Parini, S.F. Gregson, J. McCormick, D. Janse van Rensburg, T. Eibert, "Theory and Practice of Modern Antenna Range Measurements 2nd Expanded Edition, Volume 1", IET Electromagnetic Waves series 55 ISBN 978-1-83953-126-2, 2021.

[3] D. A. Hill, "A circular array for plane-wave synthesis," IEEE Trans. Electromagn. Compat., vol. 30, no. 1, pp. 3–8, Feb. 1988.

[4] Hendrik Bartko, Adam Tankielun & Benoit Derat, "New Measurements Concept of Electrically Large Active Antenna Systems in Compact Test Chambers" 8th Asia-Pacific Conference on Antennas and Propagation (APCAP 2019) August 4 – 7, 2019, Incheon, Korea.

[5] F. Scattone, et al, "Design of Dual Polarised Wide Band Plane Wave Generator for Direct Far-Field Testing" 13th European Conference on Antennas and Propagation (EuCAP 2019)

[6] F. Peng, X. Chen, H. Pei, M. Zhang, J. Zhang and Z. Ji, "Investigation of Array-based Plane Wave Generator for Compact Antenna Test Range Application," *2020 International Conference on Microwave and Millimeter Wave Technology (ICMMT)*, Shanghai, China, 2020, pp. 1-3, doi: 10.1109/ICMMT49418.2020.9386411.

[7] Z. Yang, Z. Wang, Y. Zhang and S. Gao, "Robust Plane Wave Generator Design in Small Anechoic Chamber Setup Using Parameterized Field Method," in *IEEE Access*, vol. 8, pp. 187052-187059, 2020, doi: 10.1109

[8] Y. Zhang, Z. Wang, X. Sun, Z. Qiao, W. Fan and J. Miao, "Design and Implementation of a Wideband Dual-Polarized Plane Wave Generator With Tapered Feeding Nonuniform Array," in *IEEE Antennas and Wireless Propagation Letters*, vol. 19, no. 11, pp. 1988-1992, Nov. 2020, doi: 10.1109/LAWP.2020.3010118

[9] H. Wang *et al*., "Effective Sparse Recovery Framework for Ultrawideband Robust Plane Wave Generator," in *IEEE Antennas and Wireless Propagation Letters*, vol. 22, no. 3, pp. 462-466, March 2023, doi: 10.1109/LAWP.2022.3215582

[10] H. Chen *et al*., "Synthesis of Plane-Wave Generator in 3-D Sphere Quiet Zone for Advanced Antenna Measurement by Hybridizing LSM and GA," in *IEEE Open Journal of Antennas and Propagation*, vol. 4, pp. 1044-1055, 2023, doi: 10.1109/OJAP.2023.3323812.

[11] S. Zhu, Z. Wang, W. Fan, T. -H. Loh and S. Gao, "Determining the Minimum Number of Plane Wave Generator Radiating Elements Based on SVD of the Transfer Matrix," in *IEEE Antennas and Wireless Propagation Letters*, vol. 23, no. 5, pp. 1513-1517, May 2024, doi: 10.1109/LAWP.2024.3360474

[12] O. M. Bucci, M. D. Migliore, G. Panariello and D. Pinchera, "Plane-Wave Generators: Design Guidelines, Achievable Performances and Effective Synthesis," in *IEEE Transactions on Antennas and Propagation*, vol. 61, no. 4, pp. 2005-2018, April 2013, doi: 10.1109/TAP.2012.2233453

[13] J. Wu, Y. Qi, W. Yu, L. Liu and F. Li, "An Absorber-Integrated Taper Slot Antenna," in *IEEE Transactions on Electromagnetic Compatibility*, vol. 59, no. 6, pp. 1741-1747, Dec. 2017, doi: 10.1109/TEMC.2017.2714580

[14] Z. Qiao, Z. Wang, T. -H. Loh, S. Gao and J. Miao, "A Compact Minimally Invasive Antenna for OTA Testing," in *IEEE Antennas and Wireless Propagation Letters*, vol. 18, no. 7, pp. 1381-1385, July 2019, doi: 10.1109/LAWP.2019.2917087

[15] Z. Qiao, Z. Wang, W. Fan, X. Zhang, S. Gao and J. Miao, "Low Scattering Plane Wave Generator Design Using a Novel Non-Coplanar Structure for Near-Field Over-the-Air Testing," in *IEEE Access*, vol. 8, pp. 211348-211357, 2020, doi: 10.1109/ACCESS.2020.3039367

[16] Poulton G.T. and Lim S.H. "Calculation of Input-Voltage Standing-Wave Ratio for a Reflector Antenna", IEE Electronics Letters, 14th December 1972, Vol. 8, No.25.